Check for updates

Carbon Materials | Very Important Paper

International Edition: DOI: 10.1002/anie.201814605
German Edition: DOI: 10.1002/ange.201814605

From Supramolecular Species to Self-Templated Porous Carbon and Metal-Doped Carbon for Oxygen Reduction Reaction Catalysts

*Jin Xie[+], Bo-Quan Li[+], Hong-Jie Peng[+], Yun-Wei Song, Jia-Xing Li, Ze-Wen Zhang, and Qiang Zhang**

Abstract: *The preparation of carbon materials usually involves the decomposition of precursors and the reorganization of the as-generated fragments. However, the cleavage of bonds and the simultaneous formation of new bonds at nearly the same positions prevents effective yet precise fabrication. Herein, a supramolecular precursor, cucurbit[6]uril, that contains multiple bonds with distinct bond strengths is proposed to decouple the twin problem of simultaneous bond cleavage and formation, allowing multistage transformations to hierarchical porous carbon and metal-doped carbon in a single yet effective pyrolysis step without the need of a template or additional purification. As a proof-of-concept, the Fe-doped carbon electrocatalysts realized a Pt/C-like half-wave potential of 0.869 V vs. RHE and small Tafel slope of 51.3 mV dec^{-1} in oxygen reduction reaction.*

Carbon materials is a broad family of easily accessible yet structurally tunable materials that have been widely employed in various applications, such as energy storage, adsorption, and catalysis.[1] Enormous efforts have been dedicated to their controllable synthesis toward specific structures and properties, that is, porosity and conductivity.[2] Among the preparation methods, the precursor pyrolysis approach gains the most attention owing to its simplicity and tunability.[3] Generally, this synthetic method involves the decomposition of precursors and the reorganization of as-generated fragments, concretely, the cleavage of C–C/C–H/C–X (X represents a nonmetal element) bonds and formation of new bonds (mainly sp^2 C–C bonds for graphitic carbon).[4] However, the bond cleavage/formation commonly occurs at nearly the same rate and position because of the comparable bond strengths. The simultaneous bond breaking and rebuilding always induces drastic local changes in structure and heat, resulting structural collapse of pyrolytic intermediates and final products, as well as loss of desirable features and properties (such as, high surface area, large pore volume, and heteroatom dopants).[5] Various hard and soft templates were designed to stabilize the intermediates and control the final product structure.[6] However, the cost of these templates and complicated multistep fabrication including template removal always remain a problem for applications. Hence, it is promising to develop template-free or self-templated methods toward new carbon materials and of fundamental interest to decipher the related pyrolysis mechanism.[7]

From a molecular perspective, the template-free synthesis of carbon materials relies on decoupling the twin problem of spatio-temporally identical bond cleavage and formation. In this regard, extra bonds were designed in precursors through either small-molecule crosslinking or backbone conjugation to form a rigid precursor framework.[8] Nevertheless, these attempts resulted in mostly microporous carbon that hardly contains mesopores owing to the short distance between these rigid conjunctions. If long-range interactions with bond strengths distinct from C–C/C–H/C–X bonds are included for precursor design, well-designed mesoporous or hierarchically porous carbon via template-free pyrolysis can be achieved.

Herein, supramolecular species, in which covalently bonded organic units are organized in an orderly fashion by weak intermolecular interactions, serve as the ideal precursors for controllable template-free synthesis of porous carbon (supramolecule-derived carbon, SC) and metal-doped carbon materials (SC-M, M represent a transition metal). Cucurbit[6]uril (CB6), a supramolecular compound available in crystalline form, is selected as a proof-of-concept precursor because of its highly ordered structure and extraordinary thermal stability.[9] CB6 is a bucket-like macrocyclic oligomer consist of methylene (-CH_2-) bridged glycoluril (=$C_4H_2N_4O_2$=) monomers. The glycoluril carbonyl groups allow the formation of long-range hydrogen-bonded supramolecular framework while the symmetrically distributed methylidynes are an ideal hydrocarbon precursor for graphitization. Specifically, hydrogen bonds between the carbonyl oxygen and lateral C–H groups guide a hexagonal structure with every one-dimensional (1D) micropore channel surrounded by six rows of CB6 (Figure S1). Guest molecules or ions can be easily encapsulated in these micropores with atomic dispersion, benefiting further functionalization of carbon with heteroatoms or atomically dispersed clusters.[9a]

In the as-prepared supramolecular CB6 precursor (Figure S2a), chemical bonds with various strengths are integrated, including intermolecular hydrogen bonds (several kJ mol^{-1}) and covalent bonds (70 to more than 100 kJ mol^{-1}). Consequently, as the temperature gradually increased during the pyrolysis, the cleavage and formation of each class of bonds can be spatio-temporally decoupled as thermal and

[*] J. Xie,[+] B.-Q. Li,[+] Dr. H.-J. Peng,[+] Y.-W. Song, J.-X. Li, Z.-W. Zhang, Prof. Q. Zhang
Beijing Key Laboratory of Green Chemical Reaction Engineering and Technology, Department of Chemical Engineering
Tsinghua University
Beijing 100084 (P. R. China)
E-mail: zhang-qiang@mails.tsinghua.edu.cn
[+] These authors contributed equally to this work.
Supporting information and the ORCID identification number(s) for the author(s) of this article can be found under: https://doi.org/10.1002/anie.201814605.

 © 2019 Wiley-VCH Verlag GmbH & Co. KGaA, Weinheim

spectroscopic effects suggest.[10] Below 200 °C, a dehydration and degassing process was detected with a weight loss of 7.2 %, corresponding to residual water, solvent, and HCl in the micropores (Figure 1 a).[11] From 200 to 400 °C, only a minor weight loss of 2.1 % could be detected, corresponding to some small molecules like CO and CNH fragments (Figure S3a). However, the specific thermal capacity increased simultaneously, indicating a continuous structural change within the bulk phase. The color of CB6 crystal all changed from white to yellow brown (Figure S4). This may be attributed to that at this temperature range, the weak intermolecular interactions between polar groups at the edge of CB6 become unstable and are partially cleaved to reassemble CB6 into a covalent framework through cross-linking. The main supramolecular structure remained as indicated by X-ray diffraction (XRD), while minor distortions are detected by the peak drift and broadening (Figure S5).

From 400 to 500 °C, the bulk phase began to degrade and shrink steadily, followed by a series of rearrangement of residual framework. There are two endothermic stages of weight loss, indicating a step-by-step phase transformation and conformal pore reconstitution. Synchronized MS was employed to monitor the temperature-dependent variation of gaseous fragments (Figure 1 b). These fragments include ions with m/z of 26–30, 39–43 (except 40 that represents Ar^+), 52–57, and 65–70 to represent residues with 2, 3, 4, and 5 main atoms (C, N, and O except H). At the first stage (around 450 °C), fragments with low m/z dominate, indicating $(C, N, O)_2$ species including CO^+ (m/z 28) and HCN^+ (m/z 27) as the main products. $(C, N, O)_3$ species such as $CONH^+$ (m/z 43) could also be detected (Figure S3b). These molecules are departed from the carbonyl and CH_2N groups (Figure 1 c). At the second stage, the intensities of ion fragments are relatively stronger, corresponding to the main weight loss of 44.1 %. Many larger fragments are detected, including those with 3 and 4 main atoms, such as $CONH^+$ (m/z 43) and $CONHCH_2^+$ (m/z 57), indicating the ring-opening of CB6 to volatilize N, O-rich fragments and leave C-rich backbones with reactive ends. These ends attached to each other and formed new C–C bonds (Figure S3c). The vigorous volatilization herein thinned the molecular walls within a rigid pre-formed framework, effectively resulting in uniform expansion of micropores and their merging into mesopores.

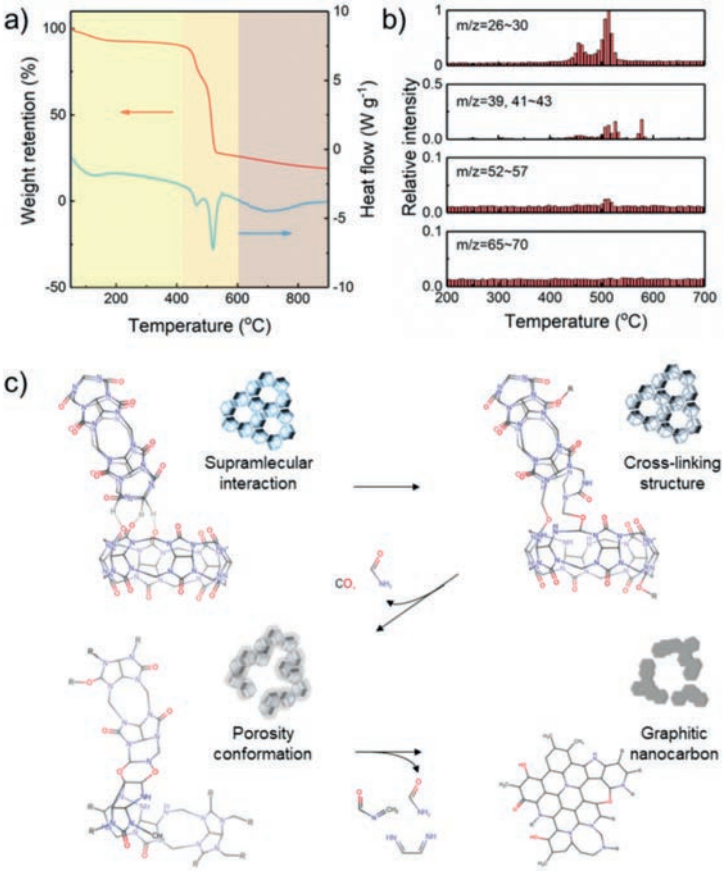

Figure 1. The pyrolysis process and mechanism for SC synthesis. a) The thermogravimetric (TG) curve and corresponding differential scanning calorimetric (DSC) profile of supramolecular CB6. b) The mass spectrometric (MS) signal of pyrolytic fragments with different mass-to-charge ratio (m/z) at different temperatures during the pyrolysis. c) Schematic illustration of the proposed multi-stage pyrolysis mechanism.

At the beginning of the final stage (after 600 °C), the material was already a carbon material that had lost the most of volatile elements. The D and G band in the Raman spectrum of the sample treated at 700 °C clearly validate the sp^2 C–C structure (Figure S6).[12] From 700 to 800 °C, the broad endothermic peak in the DSC curve (Figure 1 a), along with a narrowed Raman G band, indicates the gradual graphitization. A slightly increased intensity ratio of the D to the G band, and a major upshift of the G band from 1562 to 1581 cm^{-1} further evident the phase change from the dominant sp^2 amorphous carbon towards nanocrystalline graphitic carbon (Table S1 in the Supporting Information).[13] There is no major phase transformation and thermal effect but only a slight weight loss over 900 °C. The continues minor blue shifts in Raman G band are attributed to the constant loss of dopants under heating.[13] N_2 isotherms and corresponding pore size distribution reveals the dominant mesoporosity with a pore size of 3–8 nm (Figure 2 a, b). However, the volume of mesoporosity decreased by half for the samples treated up to from 700 to 900 °C, with a decline of the Brunauer-Emmett-Teller (BET) surface area from 1088 to 738 $m^2 g^{-1}$, indicating a slight occlusion corresponding to the graphitization during the continuous thermal treatment (Table S2). The TEM images of final product, SC, show it preserved the rhombic shape of the CB6 precursor (Figure S2b) and exhibited dominant mesoporosity that is in accordance with N_2 isotherm (Figure 2 c, d). Hence, the supramolecular approach well demonstrates an effective yet robust self-templated synthesis toward porous carbon that could be further modulated in structure and surface chemistry owing to the easy functionalization of supramolecular precursors.

 © 2019 Wiley-VCH Verlag GmbH & Co. KGaA, Weinheim

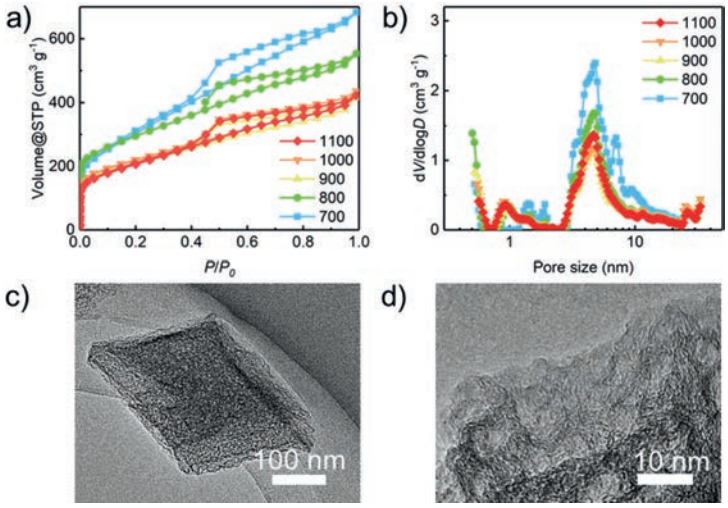

Figure 2. The mesoporosity and morphology of SC. a) The N_2 isotherm and b) corresponding pore size distribution of SC materials prepared at different temperatures [°C]. c) The TEM image and d) enlarged image of SC prepared at 900 °C.

Recently, atomically dispersed metal in carbon constitutes an important class of electrocatalysts for key applications, such as fuel cells, water splitting, and carbon dioxide fixation.[14] Compared with bulk metal catalysts, atomically dispersed metal or metal-doped carbon possesses distinct electronic structure and fully exposed active sites, rendering catalytic reactions better reactivity and selectivity.[15] Specifically, M-N-C catalysts exhibited comparable activity to commercial Pt/C electrocatalysts in oxygen reduction reaction (ORR) that is the cornerstone for fuel cell and metal-air battery applications.[16] Nevertheless, the fabrication of M-N-C is complicated and challenging as less active bulk metal and metal carbide impurities are usually presented in the product and need to be removed to fully exert high activity of M-N-C.[17] Considering the superior framework stability during pyrolysis, metal-coordinated supramolecules are expected to be an ideal precursor toward simple yet effective synthesis of high active metal-doped carbon catalysts without additional extensive purification.

To synthesize SC-Fe materials, a simple salt adsorption method was employed during precursor preparation while other synthetic steps during pyrolysis remained the same as those for SC (Figure S7–S9). Owing to the coordination with N and O heteroatoms in the CB6 framework, Fe^{2+} was atomically dispersed in the precursor. Even without acid washing, iron particle was not observed, along with the absence of crystalline signals of any iron and iron carbides in XRD patterns of SC-Fe, suggesting uniform dispersion of Fe (Figure S10 and S11). High angle annular dark-field scanning transmission electron microscope (HADDF-STEM) and N_2 isotherms reveal the uniform mesoporosity similar to SC (Figure S12 and S13). Accordingly, a tiny amount of Fe (0.23 at % according to X-ray photoelectron spectroscopy (XPS) result) has no profound influence on the pyrolysis thermodynamics (Figure S14, S15, and Table S3). High-resolution HAADF-STEM images, as well as corresponding energy dispersive spectrometric (EDS) mapping, suggest that Fe atoms are well dispersed and decorated within the carbon skeleton (Figure 3 a,b and Figure S16). The peaks in line sweeping of HAADF intensity with a width around 130 pm and synchronized EDS Fe signal well prove the atomic dispersion of Fe (Figure 3 c). These Fe species are most likely Fe atoms coordinated with nitrogen owing to the electron donation from N to Fe, which is evidenced by that 1) in the fine Fe 2p XPS spectrum of SC-Fe, the Fe $2p_{3/2}$ peak is located near Fe^{2+} (710.4 eV) instead of metallic iron (706.8 eV), and 2) in the fine N 1s XPS spectrum of SC-Fe, pyridinic nitrogen signal at 398.3 eV is enhanced and slightly blue shifted compared to SC while other peaks exhibit no major change (Figure 3 d).

The atomically uniform dispersion of Fe active sites and moderate mesoporosity endowed SC-Fe with high reactivity for ORR electrocatalysis. The ORR reactivity of the samples was evaluated using linear sweep voltammetry (LSV) conducted on a rotating ring-disk electrode in O_2-saturated 0.10 M KOH electrolyte at room temperature with an area mass loading of 0.25 mg cm^{-2} in all cases. Commercial 20 % Pt/C served as the state-of-the-art reference electrocatalyst.

Notably, all polarized profiles were calibrated with profiles tested in N_2-saturated electrolyte under otherwise identical conditions to reveal the real ORR reactivity (Fig-

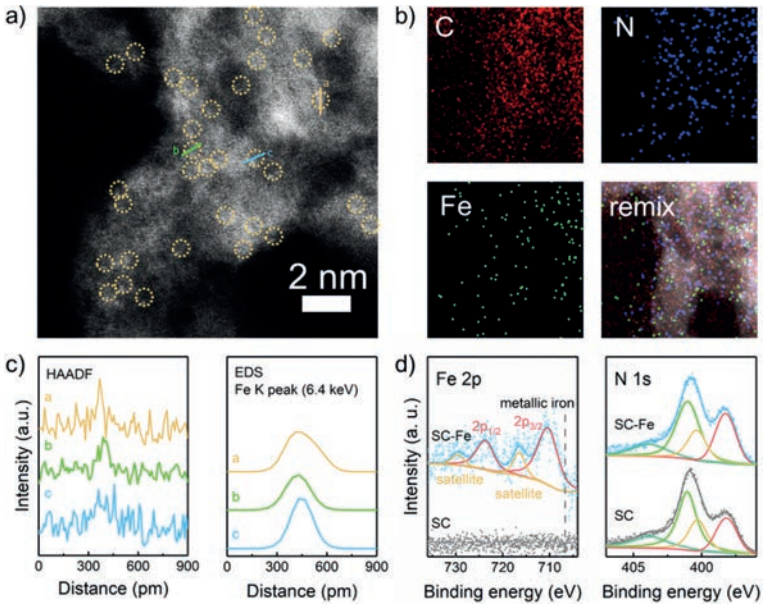

Figure 3. Atomic dispersion of metal in SC. a) The HAADF image of SC-Fe, of which partial metal atomic sites are circled, b) the EDS mapping corresponding to the HAADF image, and c) the line sweeping across a metal site (circled in (a)) of Fe K EDS signal and HAADF intensity. d) XPS Fe 2p and N 1s spectra. The peaks in N 1s spectra are assigned to pyridinic (398.3 eV), pyrrolic (400.3 eV), graphitic (401.1 eV), and oxidized nitrogen (404.0 eV), respectively.

 © 2019 Wiley-VCH Verlag GmbH & Co. KGaA, Weinheim

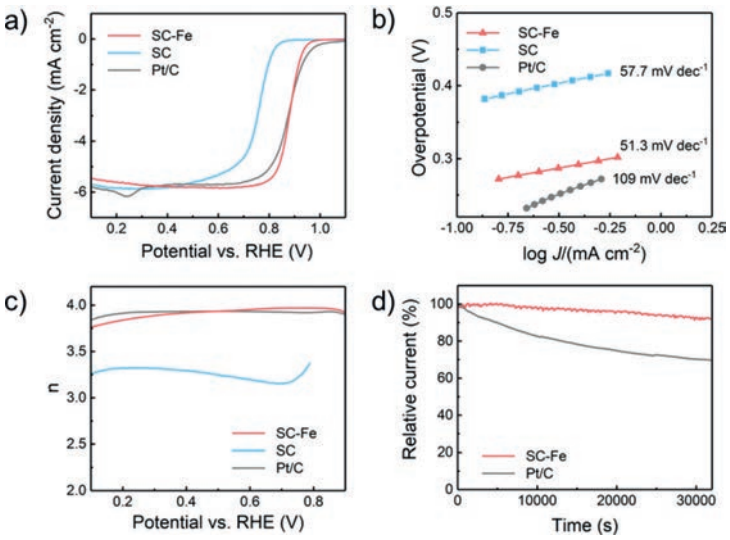

Figure 4. The electrochemical performance of SC-Fe for ORR electrocatalysis. a) LSV curves, b) Tafel slopes, and c) calculated electron transfer number of ORR of the SC-Fe, SC, and Pt/C electrocatalysts. d) Stability evaluation of the SC-Fe and Pt/C electrocatalysts.

ure S17).[18] As exhibited in Figure 4a, SC-Fe affords a half-wave potential of 0.869 V vs. reversible hydrogen electrode (RHE), which is very close to the Pt/C electrocatalyst. In contrast, the half-wave potential of SC is 100 mV lower than SC-Fe, indicating that atomically dispersed Fe is the active site for ORR. Tafel slopes afford further evidence that SC-Fe prominently promotes the ORR kinetics from 109 mV dec^{-1} for Pt/C and 57.7 mV dec^{-1} for SC to 51.3 mV dec^{-1} (Figure 4b). The electron transfer number of SC-Fe is 3.7 at 0.80 V vs. RHE and stable throughout the ORR potential range (Figure 4c and Figure S18), comparable with Pt/C and better than SC that performs a mixed ORR process to produce peroxide byproduct. In addition, long-term chronoamperometric tests suggest SC-Fe with superior ORR stability with the current density remained 90% after 30000 s at the given potential required to reach an initial ORR current density of 3.0 mA cm^{-2}, much better than the Pt/C electrocatalyst with only 70% of the current density remained (Figure 4d). Atomically dispersed SC-Fe serves as an excellent ORR electrocatalyst with comparable reactivity and better kinetics and stability than Pt/C. Supramolecular precursors such as the CB6 exhibit advantages in the preparation of atomically dispersed electrocatalysts for their 1) chemical bonds with various thermodynamic properties to arrange the pyrolysis process, 2) uniform and tunable sites for the dispersion of metal ions, 3) abundant heteroatoms to mediate the chemical environments of metal sites and interface polarity.

In conclusion, we proposed a concept of using supramolecular species to give to self-templated carbon and metal-doped carbon materials. Mechanistic insights into the pyrolysis of supramolecular CB6 suggest the key role of long-range hydrogen bonds in stabilizing the intermediate structure toward controllable template-free synthesis of hierarchical porous carbon with dominant mesoporosity. The stability of the intermediate also allowed atomic dispersion of metal atoms in the carbon framework pyrolyzed from metal-coordinated CB6, preventing the tedious purification steps and guaranteeing the full exposure of active coordinated metal sites. The as-prepared SC-Fe electrocatalyst exhibited comparable activity with Pt/C in ORR while improved kinetics and stability. This work provides the first example of the synthesis of functional carbon and metal-doped carbon from supramolecular species without templates or other complicated preparative process. The synthetic concept and pyrolysis mechanism enlighten rational design and precise fabrication of carbon and atomically dispersed metal catalysts for emerging applications.

Acknowledgements

This work was supported by National Key Research and Development Program (2016YFA0200102 and 2016YFA0202500), National Natural Science Foundation of China (21825501), and the Tsinghua University Initiative Scientific Research Program. We thank helpful discussion from Dr. Long Kong, Meng Zhao, and Prof. Jia-Qi Huang at Beijing Insitute of Technology.

Conflict of interest

The authors declare no conflict of interest.

Keywords: carbon nanomaterials · electrocatalysis · iron · oxygen reduction reaction · supramolecular precursors

How to cite: *Angew. Chem. Int. Ed.* **2019**, *58*, 4963–4967
Angew. Chem. **2019**, *131*, 5017–5021

[1] a) J. T. Zhang, C. M. Li, *Chem. Soc. Rev.* **2012**, *41*, 7016–7031; b) J. Zhang, D. S. Su, A. H. Zhang, D. Wang, R. Schlögl, C. Hebert, *Angew. Chem. Int. Ed.* **2007**, *46*, 7319–7323; *Angew. Chem.* **2007**, *119*, 7460–7464; c) E. Frackowiak, *Phys. Chem. Chem. Phys.* **2007**, *9*, 1774–1785; d) H. X. Zhong, J. Wang, Y. W. Zhang, W. L. Xu, W. Xing, D. Xu, Y. F. Zhang, X. B. Zhang, *Angew. Chem. Int. Ed.* **2014**, *53*, 14235–14239; *Angew. Chem.* **2014**, *126*, 14459–14463; e) J. Wang, H. X. Zhong, Y. L. Qin, X. B. Zhang, *Angew. Chem. Int. Ed.* **2013**, *52*, 5248–5253; *Angew. Chem.* **2013**, *125*, 5356–5361.

[2] a) J. Q. Sun, S. E. Lowe, L. J. Zhang, Y. Z. Wang, K. L. Pang, Y. Wang, Y. L. Zhong, P. R. Liu, K. Zhao, Z. Y. Tang, H. J. Zhao, *Angew. Chem. Int. Ed.* **2018**, *57*, 16511–16515; *Angew. Chem.* **2018**, *130*, 16749–16753; b) J. Wang, K. Li, H. X. Zhong, D. Xu, Z. L. Wang, Z. Jiang, Z. J. Wu, X. B. Zhang, *Angew. Chem. Int. Ed.* **2015**, *54*, 10530–10534; *Angew. Chem.* **2015**, *127*, 10676–10680.

[3] a) J. Lee, J. Kim, T. Hyeon, *Adv. Mater.* **2006**, *18*, 2073–2094; b) L. Jiao, G. Wan, R. Zhang, H. Zhou, S. H. Yu, H. L. Jiang, *Angew. Chem. Int. Ed.* **2018**, *57*, 8525–8529; *Angew. Chem.* **2018**, *130*, 8661–8665; c) R. Walczak, B. Kurpil, A. Savateev, T. Heil, J. Schmidt, Q. Qin, M. Antonietti, M. Oschatz, *Angew. Chem. Int. Ed.* **2018**, *57*, 10765–10770; *Angew. Chem.* **2018**, *130*, 10926–10931.

 © 2019 Wiley-VCH Verlag GmbH & Co. KGaA, Weinheim

[4] Y. C. Lin, J. Cho, G. A. Tompsett, P. R. Westmoreland, G. W. Huber, *J. Phys. Chem. C* **2009**, *113*, 20097 – 20107.
[5] a) M. Keiluweit, P. S. Nico, M. G. Johnson, M. Kleber, *Environ. Sci. Technol.* **2010**, *44*, 1247 – 1253; b) E. Zussman, X. Chen, W. Ding, L. Calabri, D. A. Dikin, J. P. Quintana, R. S. Ruoff, *Carbon* **2005**, *43*, 2175 – 2185.
[6] a) Z. J. Zhang, X. Y. Chen, D. H. Xie, P. Cui, J. W. Liu, *J. Mater. Chem. A* **2014**, *2*, 9675 – 9683; b) Y. H. Deng, J. Liu, C. Liu, D. Gu, Z. K. Sun, J. Wei, J. Y. Zhang, L. J. Zhang, B. Tu, D. Y. Zhao, *Chem. Mater.* **2008**, *20*, 7281 – 7286; c) C. H. Huang, R. A. Doong, D. Gu, D. Y. Zhao, *Carbon* **2011**, *49*, 3055 – 3064; d) W. Li, F. Zhang, Y. Q. Dou, Z. X. Wu, H. J. Liu, X. F. Qian, D. Gu, Y. Y. Xia, B. Tu, D. Y. Zhao, *Adv. Energy Mater.* **2011**, *1*, 382 – 386; e) Y. P. Zhai, Y. Q. Dou, X. X. Liu, S. S. Park, C. S. Ha, D. Y. Zhao, *Carbon* **2011**, *49*, 545 – 555.
[7] a) T. Chen, Z. W. Zhang, B. R. Cheng, R. P. Chen, Y. Hu, L. B. Ma, G. Y. Zhu, J. Liu, Z. Jin, *J. Am. Chem. Soc.* **2017**, *139*, 12710 – 12715; b) M. J. Li, C. M. Liu, H. B. Cao, H. Zhao, Y. Zhang, Z. J. Fan, *J. Mater. Chem. A* **2014**, *2*, 14844 – 14851; c) J. Wang, J. Tang, B. Ding, V. Malgras, Z. Chang, X. D. Hao, Y. Wang, H. Dou, X. G. Zhang, Y. Yamauchi, *Nat. Commun.* **2017**, *8*, 15717; d) X. J. Wei, S. G. Wan, S. Y. Gao, *Nano Energy* **2016**, *28*, 206 – 215; e) S. W. Bian, J. Baltrusaitis, P. Galhotra, V. H. Grassian, *J. Mater. Chem.* **2010**, *20*, 8705 – 8710; f) F. D. Han, Y. J. Bai, R. Liu, B. Yao, Y. X. Qi, N. Lun, J. X. Zhang, *Adv. Energy Mater.* **2011**, *1*, 798 – 801; g) Q. C. Zeng, D. C. Wu, C. Zou, F. Xu, R. W. Fu, Z. H. Li, Y. R. Lianga, D. S. Su, *Chem. Commun.* **2010**, *46*, 5927 – 5929; h) W. L. Zhang, H. B. Lin, Z. Q. Lin, J. Yin, H. Y. Lu, D. C. Liu, M. Z. Zhao, *ChemSusChem* **2015**, *8*, 2114 – 2122.
[8] a) J. W. F. To, Z. Chen, H. B. Yao, J. J. He, K. Kim, H. H. Chou, L. J. Pan, J. Wilcox, Y. Cui, Z. A. Bao, *ACS Cent. Sci.* **2015**, *1*, 68 – 76; b) L. J. Pan, G. H. Yu, D. Y. Zhai, H. R. Lee, W. T. Zhao, N. Liu, H. L. Wang, B. C. K. Tee, Y. Shi, Y. Cui, Z. N. Bao, *Proc. Natl. Acad. Sci. USA* **2012**, *109*, 9287 – 9292.
[9] a) S. Lim, H. Kim, N. Selvapalam, K. J. Kim, S. J. Cho, G. Seo, K. Kim, *Angew. Chem. Int. Ed.* **2008**, *47*, 3352 – 3355; *Angew. Chem.* **2008**, *120*, 3400 – 3403; b) J. Lagona, P. Mukhopadhyay, S. Chakrabarti, L. Isaacs, *Angew. Chem. Int. Ed.* **2005**, *44*, 4844 – 4870; *Angew. Chem.* **2005**, *117*, 4922 – 4949; c) J. W. Lee, S. Samal, N. Selvapalam, H. J. Kim, K. Kim, *Acc. Chem. Res.* **2003**, *36*, 621 – 630.
[10] J. G. Wang, H. Y. Jiang, N. Jiang, *Thermochim. Acta* **2009**, *496*, 136 – 142.
[11] H. Kim, Y. Kim, M. Yoon, S. Linn, S. M. Park, G. Seo, K. Kim, *J. Am. Chem. Soc.* **2010**, *132*, 12200 – 12202.
[12] a) Y. W. Zhu, H. X. Ji, H. M. Cheng, R. S. Ruoff, *Natl. Sci. Rev.* **2018**, *5*, 90 – 101; b) R. Saito, M. Hofmann, G. Dresselhaus, A. Jorio, M. S. Dresselhaus, *Adv. Phys.* **2011**, *60*, 413 – 550; c) C. X. Cong, K. Li, X. X. Zhang, T. Yu, *Sci. Rep.* **2013**, *3*, 1195.
[13] A. C. Ferrari, *Solid State Commun.* **2007**, *143*, 47 – 57.
[14] a) Y. Y. Liang, Y. G. Li, H. L. Wang, H. J. Dai, *J. Am. Chem. Soc.* **2013**, *135*, 2013 – 2036; b) H. J. Shen, E. Gracia-Espino, J. Y. Ma, K. T. Zang, J. Luo, L. Wang, S. S. Gao, X. Mamat, G. Z. Hu, T. Wagberg, S. J. Guo, *Angew. Chem. Int. Ed.* **2017**, *56*, 13800 – 13804; *Angew. Chem.* **2017**, *129*, 13988 – 13992; c) C. Y. Su, H. Cheng, W. Li, Z. Q. Liu, N. Li, Z. F. Hou, F. Q. Bai, H. X. Zhang, T. Y. Ma, *Adv. Energy Mater.* **2017**, *7*, 1602420.
[15] a) A. P. O'Mullane, *Nanoscale* **2014**, *6*, 4012 – 4026; b) J. J. Xu, D. Xu, Z. L. Wang, H. G. Wang, L. L. Zhang, X. B. Zhang, *Angew. Chem. Int. Ed.* **2013**, *52*, 3887 – 3890; *Angew. Chem.* **2013**, *125*, 3979 – 3982; c) W. H. Wang, L. Kuai, W. Cao, M. Huttula, S. Ollikkala, T. Ahopelto, A. P. Honkanen, S. Huotari, M. K. Yu, B. Y. Geng, *Angew. Chem. Int. Ed.* **2017**, *56*, 14977 – 14981; *Angew. Chem.* **2017**, *129*, 15173 – 15177; d) H. X. Zhong, J. Wang, F. L. Meng, X. B. Zhang, *Angew. Chem. Int. Ed.* **2016**, *55*, 9937 – 9941; *Angew. Chem.* **2016**, *128*, 10091 – 10095; e) Z. P. Zhang, J. T. Sun, F. Wang, L. M. Dai, *Angew. Chem. Int. Ed.* **2018**, *57*, 9038 – 9043; *Angew. Chem.* **2018**, *130*, 9176 – 9181.
[16] a) X. X. Huang, Y. Z. Wang, W. Li, Y. L. Hou, *Sci. China Chem.* **2017**, *60*, 1494 – 1507; b) W. P. Zhao, G. Wan, C. L. Peng, H. P. Sheng, J. G. Wen, H. R. Chen, *ChemSusChem* **2018**, *11*, 3473 – 3479.
[17] a) Y. J. Chen, S. F. Ji, Y. G. Wang, J. C. Dong, W. X. Chen, Z. Li, R. A. Shen, L. R. Zheng, Z. B. Zhuang, D. S. Wang, Y. D. Li, *Angew. Chem. Int. Ed.* **2017**, *56*, 6937 – 6941; *Angew. Chem.* **2017**, *129*, 7041 – 7045; b) Z. Miao, X. Wang, M.-C. Tsai, Q. Jin, J. Liang, F. Ma, T. Wang, S. Zheng, B.-J. Hwang, Y. Huang, S. Guo, Q. Li, *Adv. Energy Mater.* **2018**, *8*, 1801226.
[18] a) D. W. Wang, D. S. Su, *Energy Environ. Sci.* **2014**, *7*, 576 – 591; b) C. Tang, H. F. Wang, X. Chen, B. Q. Li, T. Z. Hou, B. S. Zhang, Q. Zhang, M. M. Titirici, F. Wei, *Adv. Mater.* **2016**, *28*, 6845 – 6851.

Manuscript received: December 25, 2018
Accepted manuscript online: January 22, 2019
Version of record online: February 15, 2019

 © 2019 Wiley-VCH Verlag GmbH & Co. KGaA, Weinheim